

Article

Synthesis and Antibacterial Aspects of Graphitic C_3N_4 @Polyaniline Composites

Mohammad Oves ^{1,*}, Mohammad Omaish Ansari ^{2,*}, Reem Darwesh ³, Afzal Hussian ⁴,
Mohamed F. Alajmi ⁴ and Huda A. Qari ⁵

¹ Center of Excellence in Environmental Studies, King Abdul-Aziz University, Jeddah 21589, Saudi Arabia

² Center of Nanotechnology, King Abdulaziz University, Jeddah 21589, Saudi Arabia

³ Physics Department, Faculty of Science, King Abdulaziz University, Jeddah 21589, Saudi Arabia; adarwesh@kau.edu.sa

⁴ Department of Pharmacognosy, College of Pharmacy, King Saud University, Riyadh 11451, Saudi Arabia; afzal.hussain.amu@gmail.com (A.H.); malajmii@ksu.edu.sa (M.F.A.)

⁵ Department of Biology, Faculty of Science, King Abdulaziz University, Jeddah 21589, Saudi Arabia; dr_hudaqari@hotmail.co.uk

* Correspondence: owais.micro@gmail.com (M.O.); omaishchem@gmail.com (M.O.A.);
Tel.: +966-509399857 (M.O.); +966-540461642 (M.O.A.)

Received: 9 September 2020; Accepted: 29 September 2020; Published: 1 October 2020



Abstract: In this work, Pani and Pani@g- C_3N_4 was synthesized by in situ oxidative polymerization methodology of aniline, in the presence of g- C_3N_4 . The as prepared Pani@g- C_3N_4 was characterized by scanning electron microscopy, transmission electron microscopy and X-ray diffraction (XRD). The morphological analysis showed well dispersed Pani in g- C_3N_4 , as well as the coating of Pani on g- C_3N_4 . The XRD further revealed this, and peaks of Pani as well as g- C_3N_4 was observed, thereby suggesting successful synthesis of the composite. The DC electrical conductivity studies under isothermal and cyclic aging conditions showed high stability of composites over 100 °C. Further, the synthesized composite material proved to be an excellent antimicrobial agent against both type i.e., gram positive *Streptococcus pneumoniae* and negative bacteria *Escherichia coli*. In the zone inhibition assay 18 ± 0.5 , 16 ± 0.75 and 20 ± 0.5 , 22 ± 0.5 mm zone diameter were found against *E. coli* and *S. pneumoniae* in presence of pure g- C_3N_4 and Pani@g- C_3N_4 at 50 μ g concentrations, respectively. Further antimicrobial activity in the presence of sunlight in aqueous medium showed that Pani@g- C_3N_4 is more potent than pure g- C_3N_4 .

Keywords: electrical conductivity; antibacterial; g- C_3N_4 ; oxidative polymerization; polyaniline

1. Introduction

With the publication of 1977 chemical communication paper by the eminent scientists' Alan J. Heeger, Alan G. MacDiarmid and Hideki Shirakawa, a new dynamic field of conducting polymers was brought into limelight [1]. Later with the discovery or utilization of other polymers such as polyaniline (Pani), polypyrrole, polythiophene, para phenylene derivatives etc., the research in this field grew by leaps and bounds. With the advent of time, the conducting polymers entered into various fields such as sensors, energy storage devices, antimicrobial materials, adsorbents for pollutants, etc. [2–5].

Among different conducting polymers, Pani has been widely used due to its properties such as: low cost of monomers, ease of polymerization, long shelf life, acid-base doping characteristics, etc. [6]. Pani has mainly been used as an antimicrobial agent against bacteria, fungi etc. [7,8]. Dhivya et al. [4] showed that the non-conduction emeraldine base of Pani is less effective against various gram-negative, gram-positive bacteria and fungus *Candida albicans* than emeraldine salt of Pani. They interpreted that

Pani binds with the cell wall and afterward, the dopant ions react with the cell, components thereby resulting in the lysis of cells. Similarly, Poyraz et al. [8] showed that Pani acts as an excellent matrix to hold silver and the composite was found to be highly effective in inhibiting the growth of *Escherichia coli* and Gram-positive *Staphylococcus pneumoniae*. Similarly, a lot of other workers have also used Pani composites successfully as antimicrobial agents [9–11]. Thus, it is established that Pani, in combination with other nanomaterials, can prove to be more lethal towards microbial growth due to the synergistic or additional effect.

Recently carbon-based materials have been widely explored for a large number of promising applications [12,13]. Among these, graphitic carbon nitride ($g\text{-C}_3\text{N}_4$) has shown promising antimicrobial properties in combination with graphene-based materials, silver etc. [14–17]. The photoactivity of $g\text{-C}_3\text{N}_4$ makes its suitable material for visible light assisted disinfection of microbial [18]. Based on the light adsorption and conductive properties of Pani along with good antimicrobial properties of $g\text{-C}_3\text{N}_4$, it is expected that their composites may show high microbial disinfection activity than the pure counterparts due to the synergism between the constituents. As the microbial activity is said to be related to the electrical conductivity which can mediate contact with the negatively charged bacterial cell surface through electrostatic adherence [19]. Thus the study of conductivity and its stability is also a factor for Pani based antimicrobial composites [20,21]. In previous studies, $g\text{-C}_3\text{N}_4$ composite material showed bactericidal activity against *E. coli* in aqueous medium under visible light illumination [22]. The bactericidal mechanism revealed the formation of light-induced holes on the $g\text{-C}_3\text{N}_4$ surface. A similar bactericidal phenomenon was also observed by applying a single layer of $g\text{-C}_3\text{N}_4$ with photo-irradiation against *E. coli* [23]. Murugesan et al. [24] showed that the composite of silver iodide anchored on $g\text{-C}_3\text{N}_4$ could prove to be an effective platform for the growth inhibition of bacteria. On further investigation, it was observed that the $\text{Ag}/g\text{-C}_3\text{N}_4$ hybrid could interact with the bacterial DNA and disturb the bacterial metabolic process.

A lot of work has been reported till date on the photocatalytic degradation of pollutants by variety of synthesized photocatalyst [25]. However, photocatalytic destruction of microorganism which also operates by similar mechanism has been poorly reported in literatures [26]. Thus, it is significant to develop light driven efficient photocatalysts for microbial destruction. This research provides new research horizons towards the use of metal-free catalysts for remarkably increased efficiency in the bacteria photoinactivation.

Thus, in this work, the composites of Pani with $g\text{-C}_3\text{N}_4$ was synthesized by in-situ oxidative polymerization of aniline with $g\text{-C}_3\text{N}_4$. The as-prepared composite was studied for its electrical conductivity properties by two aging techniques i.e., by cyclic aging conditions and isothermal aging conditions. Finally, the antibacterial properties of the composites were tested against the *E. coli* and *S. pneumoniae* and Pani@ $g\text{-C}_3\text{N}_4$ showed a much-enhanced effect than pure $g\text{-C}_3\text{N}_4$. Thus $g\text{-C}_3\text{N}_4$ based conducting polymer composites can be exciting new future materials for the disinfection of a wide variety of microorganisms.

2. Experimental

2.1. Materials

Aniline from E-Merck India Ltd. was purified by distilling under reduced pressure before use. Potassium persulphate, HCl, ethanol, melamine and Dimethyl sulfoxide (DMSO) were purchased from Sigma Aldrich and were used as received. The de-ionized water used in these experiments was obtained from a PURE ROUP 30 water purification system. Culture media nutrient broth and Agar powder was purchased from the HiMedia (Pvt. Ltd., Mumbai, India)

The culture media, solvents, antimicrobial agents, control strains and apparatus are required for the determination of minimal inhibitory concentration (MIC) test. The test was performed using Mueller-Hinton Agar (MHA), which is the most common medium for routine susceptibility

tests because it has good reproducibility and gives satisfactory growth of most bacterial pathogens. All bacterial inoculum were prepared in as heart infusion broth (HIB).

2.2. Methods and Studies

The X-ray diffraction (XRD) data were recorded with a RIGAKU-ULTIMA IV (The Woodlands, Texas, USA) with Cu Ka radiation at 1.540 \AA in the range of 10 to $90 2\theta$ at 40 kV . To study the chemical composition of the samples, X-ray photoelectron spectroscopy (XPS, New York City NY, United States) (ESCALAB 250 equipped with an Al-Ka (1486.6 eV)) with a power of 50 W and operating voltage of 1 kV was used. The surface morphological analysis was performed by field-emission scanning electron microscopy (JSM-7500F of JEOL (Tokyo, Japan) and transmission electron microscopy (FE-TEM, Tecnai G2 F20, FEI, Hillsboro, OR, USA). The DC electrical conductivity measurement under cyclic aging conditions was done using a 4-in-line probe electrical conductivity measuring instrument with a PID controlled oven (Scientific Equipments, Roorkee, India). For cyclic studies, the electrical conductivity was recorded on subsequent heating and cooling cycles from 40 – $150 \text{ }^\circ\text{C}$, while in the isothermal stability studies, the samples were subjected to 50 , 70 , 90 , 110 and $130 \text{ }^\circ\text{C}$ for 30 min and the conductivity was recorded at an interval of every 10 min . The calculation of electrical conductivity can be seen elsewhere [27].

2.3. Bacterial Disinfectant Studies of Pani@g-C₃N₄

2.3.1. Bacterial Inoculum Preparation

The pure bacterial culture of *E. coli* and *S. pneumoniae* was grown up to 16 h from the bacterial culture and was picked from the single isolated colony from the cultured medium plate. Further subculture was done in a tube with 3 mL BHI containing 0.3% yeast extract and 2% NaCl. The tube was shaken vigorously in a water bath at $30 \text{ }^\circ\text{C}$ until it achieved or exceeded the turbidity of 0.5 MacFarland standard (prepared by adding 0.5 mL of 0.048 M BaCl₂ to 99.5 mL of $0.36 \text{ NH}_2\text{SO}_4$; commercially available). The inoculum may likewise be standardized based on optical thickness (1 cm light path in a cuvette at 625 nm OD upto 0.08 – 0.1) utilizing a spectrophotometer. It is generally accomplished in 24 h and the standardized inoculum has a concentration of $1 \times 10^8 \text{ cfu/mL}$. The standardized inoculum was diluted $1:10$ in sterile normal saline solution to obtain the desired concentration of 10^6 cfu/mL and subsequently, 0.1 mL of it was taken out with the help of a pipette and transferred to well.

2.3.2. Bacterial Disinfectant Pani@g-C₃N₄ Stock Solution Preparation

The synthesized Pani@g-C₃N₄ for testing as an antimicrobial agent, immediately after synthesis was stored in the refrigerator and before experimentation (opening the cap of tubes) it was taken out to attain room temperature. The Pani@g-C₃N₄ dispersion was made by dissolving 1.0 g of it in 1 mL DMSO in order to attain a concentration of $1000 \text{ } \mu\text{g/mL}$.

2.3.3. Media Plates Preparation for Antimicrobial Assessment

The sterile petri plate was used in order to categorize the antimicrobial agent and their dose from 0 to $100 \text{ } \mu\text{g/mL}$. The petri dish was labeled on the upper portion of the bottom side in order to ensure that the plate is inserted at the correct point of the inoculating apparatus. In order to locate each bacterial strain in a well, on a reference paper, a scheme was drawn that was used to read the results. Then 1 mL of appropriate dilutions of the test antimicrobial agent was put into the labelled plate by pipette and two replicates was made for each concentration. Later 9 mL of MHA (at 48 – $50 \text{ }^\circ\text{C}$), was added into the plate with the appropriate dilution of the test antimicrobial agent and mixed thoroughly. The agar was allowed to solidify at room temperature and the plates was used immediately after the agar surface dried completely. If necessary, the surface of agar was dried in a laminar flow chamber under UV light, but excessive drying was avoided. The inoculated agar plates was kept at room temperature until the moisture in the inoculum spot was absorbed by the agar and all the spots were dry. The plates were

incubated in an inverted position at 30 °C for 24 h and after which the inoculated plate was placed on or beside the reference paper in order to identify the spot or position of each tested bacteria. The MIC was recorded at the lowest concentration of antimicrobial agent that completely inhibits the growth of the bacteria as detected by the naked eye. The control agar plates were also prepared by pipetting 10 mL of MHA into a sterile petri dish in the absence of any antimicrobial agent. In this study, the agar dilution technique was used to qualitatively measure the *in vitro* activity of an antimicrobial agent i.e., Pani@g-C₃N₄, against the test bacteria. In this method, the required amounts of Pani@g-C₃N₄ was amended in agar plates and inoculated in spots with the test microorganisms under study.

2.3.4. Zone Inhibition Assay

The modified method of the Kirby-Bauer disk diffusion susceptibility test was used to determine the sensitivity or resistance of gram-positive and negative pathogenic bacteria to Pani@g-C₃N₄. Briefly, the test strains of pathogenic bacteria were grown on Mueller-Hinton agar in the presence of different doses of Pani@g-C₃N₄ impregnated on the filter paper disks. The presence or absence of growth around the disks is an indirect measure of the ability of that compound to inhibit the growth of that organism. A 6-mm filter paper disk impregnated with a 10, 20, 40, 80 and 100 µg/disc of Pani@g-C₃N₄ were placed on a Mueller-Hinton (MH) agar plate, immediately after the inoculation of bacterial inoculum was absorbed into the plates. Here applied composite material PANI/g-C₃N₄ begun to diffuse into the surrounding agar as an antimicrobial agent. The rate of diffusion of the antimicrobial through the agar is dependent on the diffusion and solubility properties of the drug in MH agar and the molecular weight of the antimicrobial compound.

2.3.5. Bacterial Viability Assay in Light and Dark Incubation

The estimation of the viability of a bacterial culture is valuable for several environmental and medical aspects. The determination of critical threshold amount of Pani@g-C₃N₄ which affects the bacterial growth is highly useful in systematically developing the knowledge antimicrobial material. For this, variable dose treatment (0–100 µg/mL) in 5 mL culture tubes containing 1×10^6 cfu/mL was exposed to eight hours of light and eight hours in dark incubation. For confirmation of effect of treatment and light effect on bacterial cells, 0.1 ml aliquots was spread on the nutrient agar plate and incubated overnight to calculate the growing colony on the media. After overnight incubation, the bacterial growth on plate was observed and calculated. For scanning electron microscopy analysis at sub MIC concentration (50 µg/mL) growing culture was selected for the study. From each culture, 1 mL sample was centrifuged at 10,000 rpm, subsequently washed three times with phosphate saline buffer and then fixed with 2.5% glutaraldehyde at 4 °C for 8 h. After this, it was washed with 10, 20 and 30% ethanol and after that, final washing was done with Milli Q water. Each sample was attached to the grid using carbon tape and sputtered with gold layer by means of sputter coater (Quorum Q150R ES, Quorum Technologies Ltd. Ashford, Kent, UK).

2.4. Synthesis of g-C₃N₄ and Pani@g-C₃N₄ Nanocomposite

The g-C₃N₄ was synthesized from melamine by employing the methodology as reported in our earlier studies [28]. Pani@g-C₃N₄ was synthesized by insitu oxidative polymerization of aniline in the presence of g-C₃N₄. In a typical process 0.5 gm of g-C₃N₄ was dispersed in 200 mL of 1 M HCl and to which 1 mL of aniline was added under vigorous stirring conditions. To the above dispersion of g-C₃N₄ and aniline the solution of oxidant (1.48 g of Potassium persulphate in 200 mL of 1 M HCl) was added slowly to initiate polymerization. The entire setup was put under slow stirring for 24 h, after which the solution was filtered, washed with excess of water and ethanol and subsequently dedoped with ammonia solution. Thus prepared emeraldine base of Pani@g-C₃N₄ was washed again with excess of water and ethanol and finally doped with 1 M HCl. Thus prepared Pani@g-C₃N₄ nanocomposite was filtered and dried at 80 °C for 12 h and stored in desiccator for further studies.

3. Results and Discussion

3.1. Scanning Electron Microscopy

The SEM image of $g\text{-C}_3\text{N}_4$ shows a large number of strongly or loosely aggregated sheets of various sizes (Figure 1a–d). Several small particles like structure or a large number of pores on the surface are due to the gas discharge during the melamine decomposition, which resulted in the breakage of sheets and its porosity [29]. In the case of $\text{Pani}@g\text{-C}_3\text{N}_4$, surface coating of Pani occurred on $g\text{-C}_3\text{N}_4$, thereby giving $g\text{-C}_3\text{N}_4$ sheets a rough appearance and high functionality. Apart from these, tubular Pani is seen spread throughout as well as sticking or embedded in the $g\text{-C}_3\text{N}_4$ matrix. The TEM images of $\text{Pani}@g\text{-C}_3\text{N}_4$ shows the presence of $g\text{-C}_3\text{N}_4$ sheets of large dimensions. At higher magnification, Pani tubes dispersed between the sheets as well as some Pani coated on the surface can be evidently seen (Figure 2a–c).

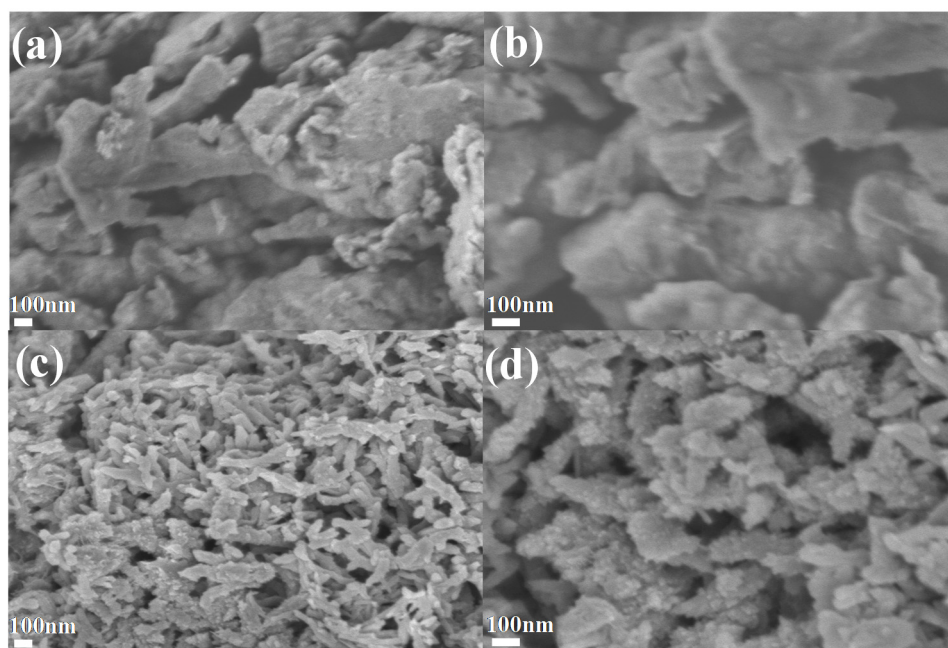


Figure 1. SEM micrographs of $g\text{-C}_3\text{N}_4$ (a,b) and $\text{Pani}@g\text{-C}_3\text{N}_4$ (c,d) at different magnifications ((a,c) is at 30,000 \times and (b,d) is at 60,000 \times magnification).

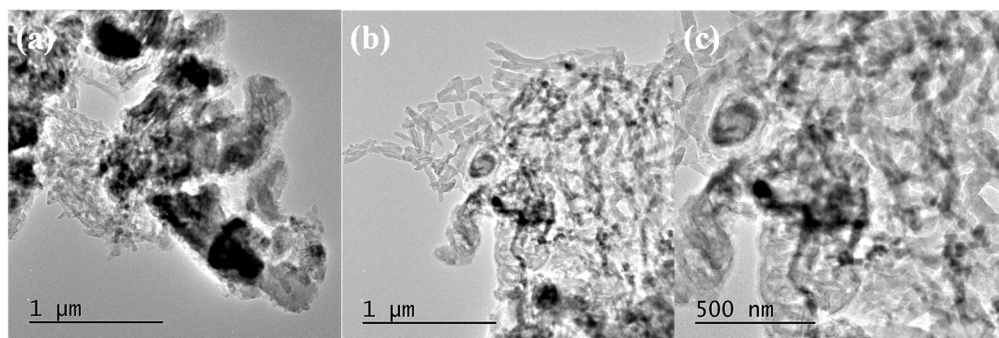


Figure 2. TEM micrographs of $\text{Pani}@g\text{-C}_3\text{N}_4$ (a–c) at different magnifications.

3.2. X-ray Diffraction

The XRD of $g\text{-C}_3\text{N}_4$ and $\text{Pani}@g\text{-C}_3\text{N}_4$ is presented in Figure 3. The XRD pattern of the synthesized $g\text{-C}_3\text{N}_4$ shows two prominent peaks at 13.2 and 27.3 2θ , which corresponds to the (100) and (002) planes of $g\text{-C}_3\text{N}_4$. The most substantial peak at 27.3 2θ is close to the peak position of graphite (002), and is due to the interlayer stacking of the conjugated aromatic systems. The small-angle peak at 13.2 2θ is associated with interlayer stacking of the tris-s-triazine unit [30]. In the case of $\text{Pani}@g\text{-C}_3\text{N}_4$ several small peaks of Pani at $\sim 9, 15, 20.5$ 2θ were observed and two large peaks at 25.6 and 27.7 2θ were observed. The noticeable difference is the reduction in the intensity of the peak in the composite, which is due to the presence of amorphous Pani as well as due to the coating of Pani on $g\text{-C}_3\text{N}_4$. Similar reduction of peak intensity has been observed for other nanomaterials on interaction with Pani [25,27].

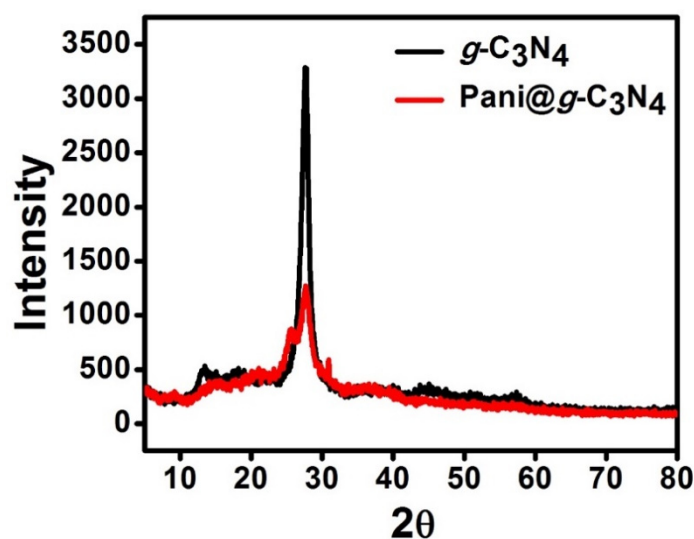
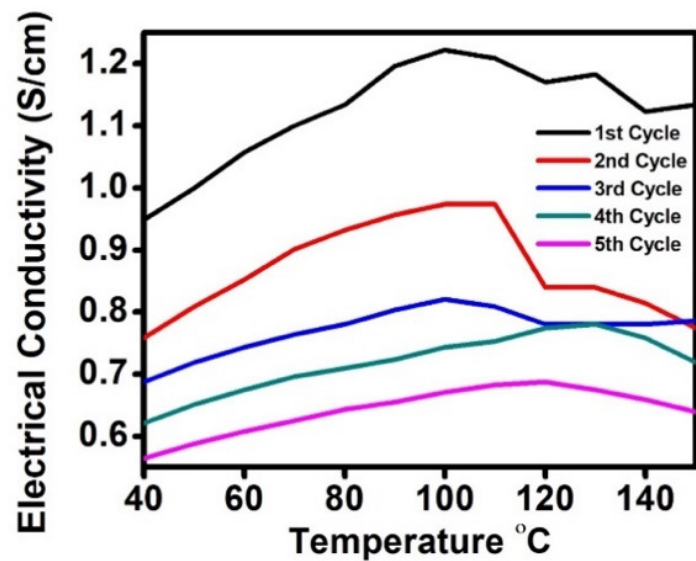


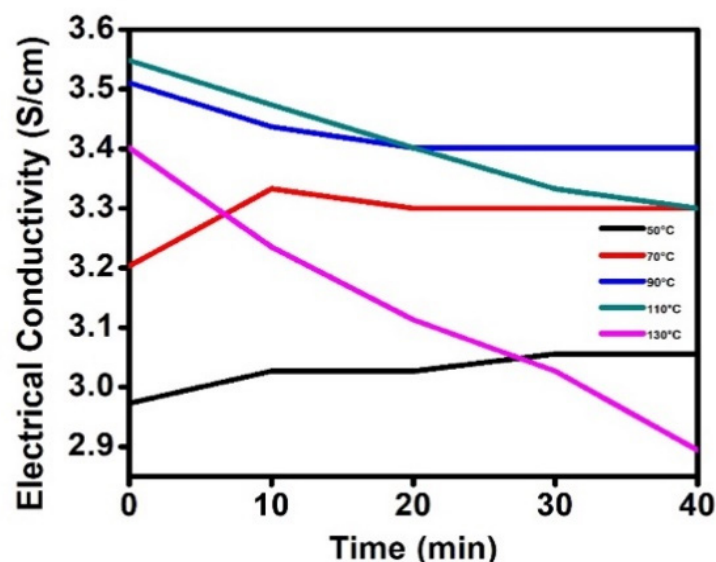
Figure 3. XRD pattern of $g\text{-C}_3\text{N}_4$ and $\text{Pani}@g\text{-C}_3\text{N}_4$.

3.3. DC Electrical Conductivity

The electrical conductivity of as-synthesized $\text{Pani}@g\text{-C}_3\text{N}_4$ at room temperature was measured to be 4.4 S/cm. After annealing the sample, the conductivity dropped to ~ 1.70 S/cm, which might be due to loss of dopant, water molecules, impurities etc. The DC electrical conductivity retention of $\text{Pani}@g\text{-C}_3\text{N}_4$ by cyclic aging studies showed an increase in electrical conductivity in each cycle. The initial conductivity dropped to lower values on each cycle, thereafter followed a rise along with the rise in temperature. It can be observed that the increase in conductivity is more uniform in the 4th and 5th cycles, which suggests that the material on subsequent annealing showed semiconducting behavior. Apart from this, in contrast to previously reported Pani based composites, here, $\text{Pani}@g\text{-C}_3\text{N}_4$ showed a slight dip in electrical conductivity after 100 °C, which might be due to highly stable $g\text{-C}_3\text{N}_4$ incorporated inside [27]. The electrical conductivity under isothermal aging conditions also showed similar behavior and stable reading were observed at 50, 70 and 90 °C; however, a dip in electrical conductivity was observed at 110 and 130 °C (Figure 4). The drop in the electrical conductivity is due to the loss of dopant, water molecules, impurities, degradation of polymer chains, etc. as mentioned above [31].



(a)



(b)

Figure 4. DC electricity conductivity retention by cyclic (a) and isothermal aging studies of Pani@g-C₃N₄ (b).

3.4. Antimicrobial Assessment

The antimicrobial assessment of g-C₃N₄ and Pani@g-C₃N₄ showed high growth inhibition against *E. coli* and *S. pneumoniae* on Petri plate which was previously amended with a specific amount of dose from 0 to 100 µg/mL. The *E. coli* growth pattern significantly diminished when applied concentration in plate was more than 75 and 60 µg/mL of g-C₃N₄ and Pani@g-C₃N₄, respectively. Similarly, *S. pneumoniae* growth disappeared at 100 µg/mL and 60 of g-C₃N₄ and Pani@g-C₃N₄, respectively, during the spot inoculation of test strain. The appearance and amount of bacterial growth on the plates depict the resistance towards g-C₃N₄ or Pani@g-C₃N₄. The bacterial growth inhibition at the minimum or lowest concentration of composite material as an antimicrobial agent is regarded as the endpoint. Similar conclusions were made previously on Pani based chemical sensor fabrication studies [32–35].

3.4.1. Zone Inhibition Assay

This study determined the antibacterial potential of $g\text{-C}_3\text{N}_4$ and $\text{Pani@g-C}_3\text{N}_4$ and the resistance pattern of gram-positive and negative pathogenic bacteria. The filter paper impregnated disk with different doses of $\text{Pani@g-C}_3\text{N}_4$ when placed on a media plate after inoculation showed excellent activity against test strain. After overnight incubation, the zone inhibition of 14 and 16 mm was found against the *E. coli*, and 15 and 18 mm zone inhibition size was found against the *S. pneumoniae* with 100 μg dose/disks of $g\text{-C}_3\text{N}_4$ and $\text{Pani@g-C}_3\text{N}_4$ applied separately (Table 1). The rate of diffusion of the antimicrobial through that the agar is dependent on the diffusion and solubility properties of the drug in agar media and the molecular weight of the antimicrobial compound. Larger molecules will diffuse at a slower rate than lower molecular weight compounds. These factors, in combination, result in antimicrobial activity having a unique breakpoint zone size indicating susceptibility to that antimicrobial compound. If the agar plate has been inoculated with a suspension of the pathogen to be tested prior to the placing of disks on the agar surface, the simultaneous growth of the bacteria and diffusion of the antimicrobial compounds occurs. Growth occurs in the presence of an antimicrobial compound when the bacteria reach a critical mass and can overpower the inhibitory effects of the antimicrobial compound. The estimated time of a bacterial suspension to reach critical mass is 8 to 10 h for most commonly recovered pathogens, but is characteristic of each species, and influenced by the media and incubation temperature. The size of the zone of inhibition of growth is influenced by the depth of the agar, since the antimicrobial diffuses in three dimensions; thus a shallow layer of agar will produce a larger zone of inhibition than a deeper layer. The point at which critical mass is reached is demonstrated by a sharply margined circle of bacterial growth around the disk. The concentration of antimicrobial compound at this margin is called the critical concentration and is approximately equal to the minimum inhibitory concentration obtained in broth dilution susceptibility tests.

Table 1. Zone of inhibition in the presence of the compound.

Microorganisms	Zone of Inhibition (mm)		
	$g\text{-C}_3\text{N}_4$	$\text{Pani@g-C}_3\text{N}_4$	Tetracycline
<i>Escherichia coli</i>	14 \pm 0.5	16 \pm 0.5	20 \pm 1.0
<i>Streptococcus pneumoniae</i>	15 \pm 0.5	18 \pm 1.0	20 \pm 1.0

Note: Zone inhibition was done at fix dose 100 μg /well on the plate in triplicate.

3.4.2. Photocatalysis Effect on Bacterial Viability

The effect of the compound in the presence of sunlight on the bacterial cell survival was checked in cfu/mL after 8 h exposure in light and dark incubation separately. Further bacterial growth patterns were confirmed by treating the sample 0.1 mL aliquots spread on the media plate subsequently incubated overnight and the appeared colony on the media has noted with significant positive results. The antibacterial activity of $g\text{-C}_3\text{N}_4$ significantly increased upto 33% in *E. coli* and 25% in *S. pneumoniae* when samples was exposed to sunlight (Table 2). While for samples treated with $\text{Pani@g-C}_3\text{N}_4$ in sunlight the antibacterial activity was 50 and 58% against *E. coli* and *S. pneumoniae*, respectively (figure bacteria Sem). Overall it was concluded that the antibacterial activity of $g\text{-C}_3\text{N}_4$ and $\text{Pani@g-C}_3\text{N}_4$ was significantly enhanced on being exposed to sunlight. Similarly, effect of photocatalysis on the bacterial diversity was observed previously [36,37]. The photoinactivation of *E. coli* and *S. pneumoniae* by $g\text{-C}_3\text{N}_4$ $\text{Pani@g-C}_3\text{N}_4$ thin film can be explained by first adsorption of $g\text{-C}_3\text{N}_4$ $\text{Pani@g-C}_3\text{N}_4$ to the negatively charged bacterial cell surface through electrostatic adherence. The absorption of visible light by $g\text{-C}_3\text{N}_4$ and $\text{Pani@g-C}_3\text{N}_4$ produces e^-/h^+ pairs. The e^-/h^+ pairs by a series of reactions generates OH radical which are responsible for the photoinactivation of bacterial. Firstly, the radicals damage the surfaces of the bacterial cells leading to the leaking of internal components through the damaged sites which eventually leads to the death of bacterial cells [38]. This is evident from the SEM micrographs as shown in Figure 5.

Table 2. Minimum inhibition concentration of compound in absence and presence of sunlight.

Microorganisms	Minimum Inhibitory Concentration (MIC)			
	$g\text{-C}_3\text{N}_4$		Pani@ $g\text{-C}_3\text{N}_4$	
	Dark	Sunlight	Dark	Sunlight
<i>Escherichia coli</i>	75	50	60	30
<i>Streptococcus pneumoniae</i>	100	75	60	25

Note: Both experiments separately done in dark and light condition.

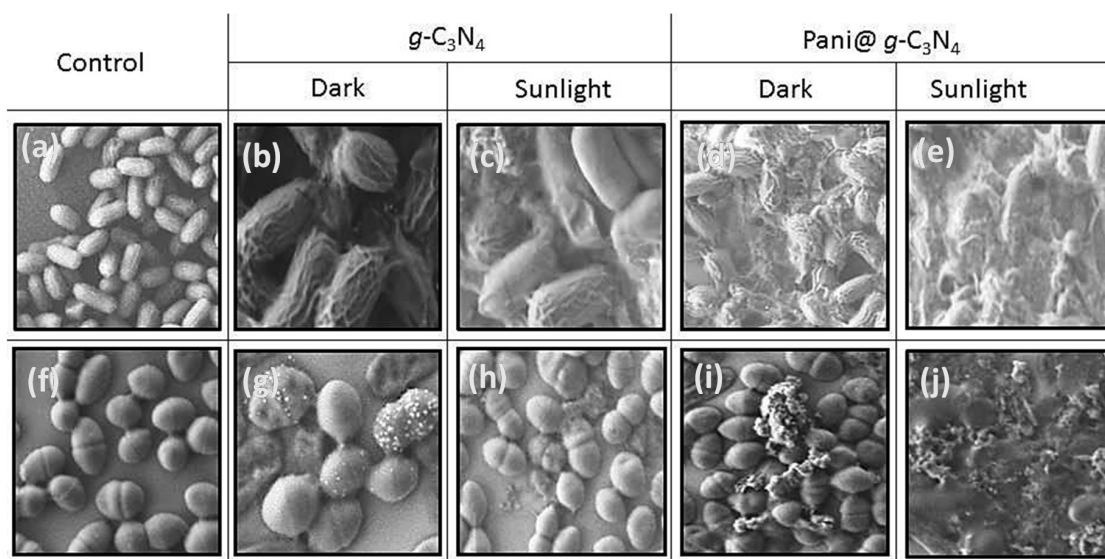


Figure 5. The effect of $g\text{-C}_3\text{N}_4$ and Pani@ $g\text{-C}_3\text{N}_4$ on *E. coli* and *S. pneumoniae* cells structure in dark and sunlight. The micrographs labeled (a) and (f) are control *E. coli* and *S. pneumoniae* respectively; (b) and (g) are $g\text{-C}_3\text{N}_4$ treated *E. coli* and *S. pneumoniae* in dark respectively; (c) and (h) are $g\text{-C}_3\text{N}_4$ treated *E. coli* and *S. pneumoniae* in sunlight respectively; (d) and (i) are Pani@ $g\text{-C}_3\text{N}_4$ treated *E. coli* and *S. pneumoniae* in dark respectively while (e) and (j) are Pani@ $g\text{-C}_3\text{N}_4$ treated *E. coli* and *S. pneumoniae* in sunlight respectively.

4. Conclusions

In summary, the successful synthesis of Pani@ $g\text{-C}_3\text{N}_4$ composites has been achieved by simple in-situ oxidative polymerization of aniline along with $g\text{-C}_3\text{N}_4$. The coating of Pani on $g\text{-C}_3\text{N}_4$ was confirmed by SEM and TEM, which suggested strong interaction between them. Pani@ $g\text{-C}_3\text{N}_4$ showed high DC electrical conductivity retention at elevated temperatures under isothermal and cyclic aging conditions, which might be due to highly stable $g\text{-C}_3\text{N}_4$, thereby resisting the degradation of Pani, by dissipating heat, synergistic effect etc. Furthermore, the excellent antimicrobial activity of Pani@ $g\text{-C}_3\text{N}_4$ when applied in the presence of sunlight against the indicator organism *E. coli* and pathogenic bacterial strain of *Streptococcus pneumoniae* suggested its applications towards environmental remediation applications.

Author Contributions: Conceptualization, M.O. and M.O.A.; methodology, M.O. and M.O.A.; software, R.D.; validation, A.H., M.F.A. and H.A.Q.; formal analysis, A.H.; investigation, M.O.; resources, M.O.A.; data curation, M.O.; writing—original draft preparation, M.O. and M.O.A.; writing—review and editing, A.H.; visualization, H.A.Q.; supervision, M.O.A.; project administration, A.H.; funding acquisition, M.F.A. All authors have read and agreed to the published version of the manuscript.

Funding: This research received no external funding.

Acknowledgments: The authors greatly acknowledge to the Centre of Excellence environmental studies and Center of Nanotechnology, King Abdulaziz University, Jeddah, Makkah, KSA. The authors also greatly acknowledge the generous support from Researchers Supporting Project number (RSP-2020-122), King Saud University, Riyadh, Saudi Arabia.

Conflicts of Interest: The authors declare no conflict of interest.

References

1. Shirakawa, H.; Louis, E.J.; MacDiarmid, A.G.; Chiang, C.K.; Heeger, A.J. Synthesis of electrically conducting organic polymers: Halogen derivatives of polyacetylene, $(\text{CH})_x$. *J. Chem. Soc. Chem. Commun.* **1977**, 578–580. [[CrossRef](#)]
2. Ansari, M.O.; Mohammad, F. Thermal stability, electrical conductivity and ammonia sensing studies on p-toluenesulfonic acid doped polyaniline:titanium dioxide (pTSA/Pani:TiO₂) nanocomposites. *Sens. Actuators B-Chem.* **2011**, *157*, 122–129. [[CrossRef](#)]
3. Ansari, M.O.; Kumar, R.; Ansari, S.A.; Ansari, S.P.; Barakat, M.A.; Alshahrie, A.; Cho, M.H. Anion selective pTSA doped polyaniline@graphene oxide-multiwalled carbon nanotube composite for Cr(VI) and Congo red adsorption. *J. Colloid Interface Sci.* **2017**, *496*, 407–415. [[CrossRef](#)] [[PubMed](#)]
4. Dhivya, C.; Vandarkuzhali, S.A.A.; Radha, N. Antimicrobial activities of nanostructured polyanilines doped with aromatic nitro compounds. *Arab. J. Chem.* **2019**, *12*, 3785–3798. [[CrossRef](#)]
5. Kumar, R.; Ansari, M.O.; Alshahrie, A.; Darwesh, R.; Parveen, N.; Yadav, S.K.; Barakat, M.A.; Cho, M.H. Adsorption modeling and mechanistic insight of hazardous chromium on para toluene sulfonic acid immobilized-polyaniline@CNTs nanocomposites. *J. Saudi Chem. Soc.* **2019**, *23*, 188–197. [[CrossRef](#)]
6. Ansari, M.O.; Oves, M.; Salah, N.; Asad, M.; Kumar, R.; Hasan, P.M.Z.; Alshahrie, A.; Darwesh, R. DC electrical conductivity retention and antibacterial aspects of microwave-assisted ultrathin CuO@polyaniline composite. *Chem. Pap.* **2020**, *74*, 3887–3898. [[CrossRef](#)]
7. Ahmad, N.; Sultana, S.; Kumar, G.; Zuhaib, M.; Sabir, S.; Khan, M.Z. Polyaniline based hybrid bionanocomposites with enhanced visible light photocatalytic activity and antifungal activity. *J. Environ. Chem. Eng.* **2019**, *7*, 102804. [[CrossRef](#)]
8. Poyraz, S.; Cerkez, I.; Huang, T.S.; Liu, Z.; Kang, L.; Luo, J.; Zhang, X. One-step Synthesis and Characterization of Polyaniline Nanofiber/Silver Nanoparticle Composite Networks as Anti-bacterial Agents. *ACS Appl. Mater. Interface* **2014**, *6*, 20025–20034. [[CrossRef](#)]
9. Farias, E.A.O.; Dionisio, N.A.; Quelemes, P.V.; Sergio, H.L.; José, M.E.M.; Edson, C.S.F.; Ivan, H.B.; José Roberto, S.A.L.; Carla, E. Development and characterization of multilayer films of polyaniline, titanium dioxide and CTAB for potential antimicrobial applications. *Mater. Sci. Eng. C* **2014**, *35*, 449–454. [[CrossRef](#)]
10. Hussein, M.A.; El-Shishtawy, R.M.; Alamry, K.A.; Asiri, A.M.; Mohamed, S.A. Efficient water disinfection using hybrid polyaniline/graphene/carbon nanotube nanocomposites. *Environ. Technol.* **2019**, *40*, 2813–2824. [[CrossRef](#)]
11. Mohsen, R.M.; Morsi, S.M.M.; Selim, M.M.; Ghoneim, A.M.; El-Sherif, H.M. Electrical, thermal, morphological, and antibacterial studies of synthesized polyaniline/zinc oxide nanocomposites. *Polym. Bull.* **2019**, *76*, 1–21. [[CrossRef](#)]
12. Almoisheer, N.; Alseroury, F.A.; Kumar, R.; Almeelbi, T.; Barakat, M.A. Synthesis of Graphene Oxide/Silica/Carbon Nanotubes Composite for Removal of Dyes from Wastewater. *Earth Syst. Environ.* **2019**, *3*, 651–659. [[CrossRef](#)]
13. Kumar, R.; Laskar, M.A.; Hewaidy, I.F.; Barakat, M.A. Modified Adsorbents for Removal of Heavy Metals from Aqueous Environment: A Review. *Earth Syst. Environ.* **2019**, *3*, 83–93. [[CrossRef](#)]
14. Liu, C.; Wang, L.; Xu, H.; Wang, S.; Gao, S.; Ji, X.; Xu, Q.; Lan, W. “One pot” green synthesis and the antibacterial activity of g-C₃N₄/Ag nanocomposites. *Mater. Lett.* **2016**, *164*, 567–570. [[CrossRef](#)]
15. Sun, L.; Du, T.; Hu, C.; Chen, J.; Lu, J.; Lu, Z.; Han, H. Antibacterial Activity of Graphene Oxide/g-C₃N₄ Composite through Photocatalytic Disinfection under Visible Light. *ACS Sustain. Chem. Eng.* **2017**, *5*, 8693–8701. [[CrossRef](#)]
16. Qamar, M.A.; Shahid, S.; Javed, M.; Iqbal, S.; Sher, M.; Akbar, M.B. Highly efficient g-C₃N₄/Cr-ZnO nanocomposites with superior photocatalytic and antibacterial activity. *J. Photochem. Photobiol. Chem.* **2020**, *401*, 112776. [[CrossRef](#)]

17. Thakur, D.; Ta, Q.T.H.; Noh, J.S. Photon-Induced Superior Antibacterial Activity of Palladium-Decorated, Magnetically Separable Fe₃O₄/Pd/mpg-C₃N₄ Nanocomposites. *Molecules* **2019**, *24*, 3888. [[CrossRef](#)]
18. Ngullie, R.C.; Alaswad, S.O.; Bhuvaneshwari, K.; Shanmugam, P.; Pazhanivel, T.; Arunachalam, P. Synthesis and Characterization of Efficient ZnO/g-C₃N₄ Nanocomposites Photocatalyst for Photocatalytic Degradation of Methylene Blue. *Coatings* **2020**, *10*, 500. [[CrossRef](#)]
19. Robertson, J.; Nikolaidis, M.G.; Nieuwoudt, M.K.; Swift, S. The antimicrobial action of polyaniline involves production of oxidative stress while functionalisation of polyaniline introduces additional mechanisms. *PeerJ* **2018**, *6*, e5135. [[CrossRef](#)]
20. Nikolaidis, M.R.G.; Bennett, J.R.; Swift, S.; Easteal, A.J.; Ambrose, M. Broad spectrum antimicrobial activity of functionalized polyanilines. *Acta Biomater.* **2011**, *2*, 4204–4209. [[CrossRef](#)]
21. Zengin, H.; Aksin, G.; Zengin, G.; Kahraman, M.; Kilic, I.H. Preparation and Characterization of Conductive Polyaniline/Silver Nanocomposite Films and Their Antimicrobial Studies. *Polym. Eng. Sci.* **2019**, *59*, E182–E194. [[CrossRef](#)]
22. Huang, J.; Ho, W.; Wang, X. Metal-free disinfection effects induced by graphitic carbon nitride polymers under visible light illumination. *Chem. Comm.* **2014**, *50*, 4338–4340. [[CrossRef](#)] [[PubMed](#)]
23. Zhao, H.; Yu, H.; Quan, X.; Chen, S.; Zhang, Y.; Zhao, H.; Wang, H. Fabrication of atomic single layer graphitic-C₃N₄ and its high performance of photocatalytic disinfection under visible light irradiation. *Appl. Catal. B Environ.* **2014**, *152*, 46–50. [[CrossRef](#)]
24. Murugesan, P.; Narayanan, S.; Matheswaran, M. Photocatalytic performance and antibacterial activity of visible light driven silver iodide anchored on Graphitic-C₃N₄ binary composite. *Environ. Nanotechnol. Monit. Manag.* **2018**, *10*, 253–263. [[CrossRef](#)]
25. Kumar, R.; Barakat, M.A.; Alseroury, F.A. Oxidized g-C₃N₄/polyaniline nanofiber composite for the selective removal of hexavalent chromium. *Sci. Rep.* **2017**, *7*, 1–11. [[CrossRef](#)] [[PubMed](#)]
26. Barakat, M.A.; Anjum, M.; Kumar, R.; Alafif, Z.; Oves, M.; Ansari, M.O. Design of ternary Ni(OH)₂/graphene oxide/TiO₂ nanocomposite for enhanced photocatalytic degradation of organic, microbial contaminants, and aerobic digestion of dairy wastewater. *J. Clean. Prod.* **2020**, *258*, 120588. [[CrossRef](#)]
27. Ansari, M.O.; Mohammad, F. Thermal stability of HCl-doped-polyaniline and TiO₂ nanoparticles-based nanocomposites. *J. Appl. Polym. Sci.* **2012**, *124*, 4433–4442. [[CrossRef](#)]
28. Alshahrie, A.; Ansari, M.O. High Performance Supercapacitor Applications and DC Electrical Conductivity Retention on Surfactant Immobilized Macroporous Ternary Polypyrrole/Graphitic-C₃N₄@Graphene Nanocomposite. *Electron. Mater. Lett.* **2019**, *15*, 238–246. [[CrossRef](#)]
29. Yuan, X.; Zhou, C.; Jing, Q.; Tang, Q.; Mu, Y.; Du, A. Facile Synthesis of g-C₃N₄ Nanosheets/ZnO Nanocomposites with Enhanced Photocatalytic Activity in Reduction of Aqueous Chromium(VI) under Visible Light. *Nanomaterials* **2016**, *6*, 173. [[CrossRef](#)]
30. Tahir, M.; Cao, C.; Butt, F.K.; Butt, S.; Idrees, F.; Ali, Z.; Aslam, I.; Tanveer, M.; Mahmood, A.; Mahmood, N. Large scale production of novel g-C₃N₄ micro strings with high surface area and versatile photodegradation ability. *CrystEngComm* **2014**, *16*, 1825–1830. [[CrossRef](#)]
31. Ansari, M.O.; Kumar, R.; Alshahrie, A.; Abdel-wahab, M.S.; Sajith, V.K.; Ansari, M.S.; Jilani, A.; Barakat, M.A.; Darwesh, R. CuO sputtered flexible polyaniline@graphene thin films: A recyclable photocatalyst with enhanced electrical properties. *Compos. B Eng.* **2019**, *175*, 107092. [[CrossRef](#)]
32. Oves, M.; Shahadat, M.; Ansari, S.A.; Aslam, M.; Ismail, I.I.M. Polyaniline Nanocomposite Materials for Biosensor Designing, Electrically Conductive Polymer and Polymer Composites. In *Book Synthesis to Biomedical Applications*; Khan, A., Jawaid, M., Khan, A.A.P., Asiri, A.M., Eds.; Wiley-VCH Verlag: Weinheim, Germany, 2018; pp. 113–135.
33. Khan, A.A.P.; Khan, A.; Rahman, M.M.; Asiri, A.M.; Oves, M. Chemical sensor development and antibacterial activities based on polyaniline/gemini surfactants for environmental safety. *J. Polym. Environ.* **2018**, *26*, 1673–1684. [[CrossRef](#)]
34. Thakur, B.; Amarnath, C.A.; Mangoli, S.H.; Sawant, S.N. Polyaniline nanoparticle based colorimetric sensor for monitoring bacterial growth. *Sens. Actuators B Chem.* **2015**, *207*, 262–268. [[CrossRef](#)]

35. Bushra, R.; Shahadat, M.; Ahmad, A.; Nabi, S.A.; Umar, K.; Oves, M.; Raeissi, A.S.; Muneer, M. Synthesis, characterization, antimicrobial activity and applications of polyanilineTi (IV) arsenophosphate adsorbent for the analysis of organic and inorganic pollutants. *J. Hazard. Mater.* **2014**, *264*, 481–489. [[CrossRef](#)] [[PubMed](#)]
36. Faraji, M.; Mohaghegh, N.; Abedini, A. Ternary composite of TiO₂ nanotubes/Ti plates modified by g-C₃N₄ and SnO₂ with enhanced photocatalytic activity for enhancing antibacterial and photocatalytic activity. *J. Photochem. Photobiol. B Biol.* **2018**, *178*, 124–132. [[CrossRef](#)] [[PubMed](#)]
37. Bushra, R.; Arfin, T.; Oves, M.; Raza, W.; Mohammad, F.; Khan, M.A.; Ahmad, A.; Ameer, A.; Muneer, M. Development of PANI/MWCNTs decorated with cobalt oxide nanoparticles towards multiple electrochemical, photocatalytic and biomedical application sites. *New J. Chem.* **2016**, *40*, 9448–9459. [[CrossRef](#)]
38. Koli, V.B.; Delekar, S.D.; Pawar, S.H. Photoinactivation of bacteria by using Fe-doped TiO₂-MWCNTs nanocomposites. *J. Mater. Sci. Mater. Med.* **2016**, *27*, 177. [[CrossRef](#)]



© 2020 by the authors. Licensee MDPI, Basel, Switzerland. This article is an open access article distributed under the terms and conditions of the Creative Commons Attribution (CC BY) license (<http://creativecommons.org/licenses/by/4.0/>).